

Supplementary Materials for

Filling-enforced quantum band insulators in spin-orbit coupled crystals

Hoi Chun Po, Haruki Watanabe, Michael P. Zaletel, Ashvin Vishwanath

Published 8 April 2016, *Sci. Adv.* **2**, e1501782 (2016)

DOI: 10.1126/sciadv.1501782

The PDF file includes:

- Electron filling in AIs
- Symmetries of SG No. 199
- feQBI tight-binding examples
- Hypothetical structure for spin-orbit coupled hyperkagome material $\text{Na}_3\text{Ir}_3\text{O}_8$
- Discussions on the SE cut
- Fig. S1. Reproduction of Fig. 1D with different viewing conditions and extra annotation.
- Fig. S2. Energy and entanglement band structure for an alternative feQBI example for SG No. 199.
- Fig. S3. Plot of band gap for the hyperkagome model in eq. S3 at filling $\nu = 4$.
- Fig. S4. Plot of surface band structure against the surface crystal momentum \vec{k}_{\parallel} for the model in eq. S3.
- Table S1. List of symmetry elements for SG No. 199.
- Table S2. Spin-quantization axes corresponding to the SG symmetric spin texture.
- Table S3. Symmetry eigenvalues of the irreducible little group representations at high-symmetry momenta.
- Table S4. Transformation of tight-binding sites under the symmetry elements.
- Table S5. A full list of terms in the feQBI tight-binding example given in the text.
- Table S6. Terms in an alternative eight-band feQBI tight-binding example.
- Table S7. Measured structure of $\text{Na}_3\text{Ir}_3\text{O}_8$ by Takayama *et al.* (19).
- Table S8. “Symmetry-enriched” hypothetical structure of $\text{Na}_3\text{Ir}_3\text{O}_8$ in SG No. 214.

Electron filling in AIs

Here we discuss how to determine the electron fillings consistent with atomic insulators.

Given an SG \mathcal{G} , symmetry-related points are grouped under the 'Wyckoff positions' $\mathcal{W}_w^{\mathcal{G}}$, where the 'Wyckoff letters' w ($= a, b, \dots$) label qualitatively distinct set of points. We denote by $|\mathcal{W}_w^{\mathcal{G}}|$ the number of symmetry-related points in each primitive unit cell corresponding to $\mathcal{W}_w^{\mathcal{G}}$.

The AI fillings compatible with an SG \mathcal{G} and TR take the form $\nu^{\text{AI}} = 2 \sum_{\{w\}} |\mathcal{W}_w^{\mathcal{G}}|$, where the sum is over a set of Wyckoff positions $\{w\}$. The minimum filling for an AI is hence

$\nu_{\text{min}}^{\text{AI}} = 2 |\mathcal{W}_a^{\mathcal{G}}|$. Symmorphic crystals always have $|\mathcal{W}_a^{\mathcal{G}}| = 1$ and therefore $\nu_{\text{min}}^{\text{AI}} = 2$, which must coincide with $\nu_{\text{min}}^{\text{BI}}$ due to Kramers degeneracy. When \mathcal{G} is non-symmorphic, $|\mathcal{W}_a^{\mathcal{G}}|$ is SG-dependent but it is always ≥ 2 , giving $\nu_{\text{min}}^{\text{AI}} \geq 4$. $\mathcal{W}_w^{\mathcal{G}}$ for the four Wyckoff-mismatched SGs are listed Ref. (5) and are reproduced in Table 1 of the main text. One sees that $\nu_{\text{min}}^{\text{AI}} = 8, 8, 12$ and 16 for SGs No. 199, 214, 220 and 230 respectively.

Next we argue a valence bond solid (VBS) arising from one spin-1/2 moment localized on each site of a SG-symmetric lattice either has an electron filling consistent with an AI, or breaks SG symmetries. Assume the VBS respects SG symmetries. Let \vec{r} and \vec{r}' be the coordinates of two spin-1/2 moments paired into a spin-singlet state. By assumption any SG symmetry g either moves both \vec{r} and \vec{r}' (generating another valence bond), or leaves both invariant. In both cases, the system remains SG symmetric under the linear scaling of the valence bond by a factor t : $\vec{r} \rightarrow \vec{\bar{r}} + t(\vec{r} - \vec{r}')/2$ and $\vec{r}' \rightarrow \vec{\bar{r}} + t(\vec{r}' - \vec{r})/2$, where $\vec{\bar{r}} = (\vec{r} + \vec{r}')/2$ is the bond center. In particular, $t=0$ corresponds to localizing both spins in the valence bond to the same site $\vec{\bar{r}}$, reproducing an AI.

To illustrate the idea we discuss below two concrete examples. First consider a 2D rectangular lattice with a glide symmetry $(x, y) \rightarrow (x+1/2, -y)$. The SG-symmetric lattice generated by the site (a, b) contains two sites in each unit cell, with the other site at $(a+1/2, -$

b). (Note the abuse of notation: in these 2D setups we let 'SG' stand for wallpaper group instead of space group). For this system the AI fillings are $\nu^{\text{AI}} \in 4\mathbb{N}$. Now suppose the system is at filling $\nu = 2 < 4$, with one electron localized on each site of the mentioned lattice. To respect time-reversal symmetry, one can attempt to pair the two spin-1/2 moments in the unit cell into a singlet state. Under the glide symmetry, however, the singlet bond changes from intra- to inter-cell, and therefore the considered VBS state breaks SG symmetries.

As another example, consider replacing the glide reflection by a regular reflection symmetry $(x, y) \rightarrow (x, -y)$. Since the point $(a, 0)$ is taken back to itself under the mirror, a minimum of one site in each unit cell is sufficient to respect the SG symmetries, giving AI fillings $\nu^{\text{AI}} \in 2\mathbb{N}$. Now suppose again we are at filling $\nu = 2$, with two spin-1/2 moments localized on each of the two symmetry-related sites (a, b) and $(a, -b)$ in the unit cell. This time, the valence bond between these two spins does not break any symmetries. Indeed, one sees that it is possible to smoothly deform the lattice and take $b \rightarrow 0$, reducing the VBS state to a strict AI.

Symmetries of SG No. 199

In this appendix we provide supplementary information on the symmetry properties of SG No. 199, an explicit tabulation of the feQBI tight-binding example discussed in Eq. 1 of main text, and also an additional tight-binding example.

SG No. 199 has three Wyckoff positions labeled by a, b and c, which can respectively be realized by having 4, 6 and 12 sites in each primitive unit cell. In particular, the hyperkagome lattice in Fig. 1d of the main text corresponds to a lattice in \mathcal{W}_6^{199} . To aid visualization, we present in fig. S1 views of the lattice from different angles.

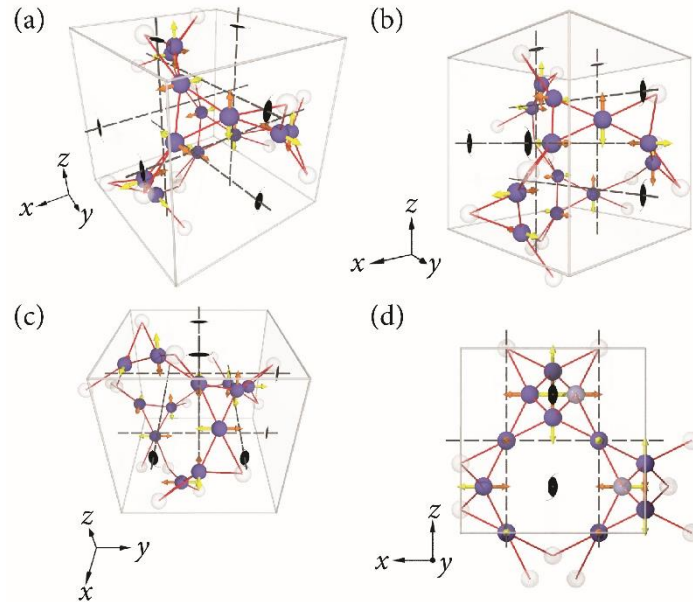


fig. S1. Reproduction of Fig. 1D with different viewing conditions and extra annotation. The screw axes are also included, indicated by dashed lines. On each site, the colored double-headed arrows indicate the direction of the site-dependent spin-quantization axes for the SG-symmetric spin-texture.

Symmetries elements

Up to lattice translations, No. 199 contains 12 symmetry elements. We parameterize the SG element g by $g = \{R_g = Ie^{-i\vec{\theta}_g \cdot \vec{L}} | \vec{t}_g\}$, where $I = +1$ (-1) for proper (improper) rotation. While these can be easily determined from the information listed in ITC (5), we tabulate them in table S1 for completeness ('el' denotes the symmetry operation indexed by the same number in ITC).

table S1. List of symmetry elements for SG No. 199. Elements are parameterized by

$$g = \{R_g = Ie^{-i\vec{\theta}_g \cdot \vec{L}} | \vec{t}_g \}.$$

el.	I	$\vec{\theta}_g$	\vec{t}_g
(1)	+	(0, 0, 0)	(0, 0, 0)
(2)	+	$\pi(0, 0, 1)$	(1/2, 0, 1/2)
(3)	+	$\pi(0, 1, 0)$	(0, 1/2, 1/2)
(4)	+	$\pi(1, 0, 0)$	(1/2, 1/2, 0)
(5)	+	$\frac{2\pi}{3} \frac{1}{\sqrt{3}}(1, 1, 1)$	(0, 0, 0)
(6)	+	$\frac{2\pi}{3} \frac{1}{\sqrt{3}}(-1, 1, -1)$	(1/2, 1/2, 0)
(7)	+	$\frac{2\pi}{3} \frac{1}{\sqrt{3}}(1, -1, -1)$	(1/2, 0, 1/2)
(8)	+	$\frac{2\pi}{3} \frac{1}{\sqrt{3}}(-1, -1, 1)$	(0, 1/2, 1/2)
(9)	+	$\frac{4\pi}{3} \frac{1}{\sqrt{3}}(1, 1, 1)$	(0, 0, 0)
(10)	+	$\frac{4\pi}{3} \frac{1}{\sqrt{3}}(1, -1, -1)$	(0, 1/2, 1/2)
(11)	+	$\frac{4\pi}{3} \frac{1}{\sqrt{3}}(-1, -1, 1)$	(1/2, 1/2, 0)
(12)	+	$\frac{4\pi}{3} \frac{1}{\sqrt{3}}(-1, 1, -1)$	(1/2, 0, 1/2)

Space-group-symmetric spin-texture

Our notion of a SG-symmetric spin-orbital entanglement cut requires the existence of SG-symmetric spin-texture, i.e. an assignment of polarized spin states on each site of the lattice that does not break any of the SG symmetries. In this subsection we elaborate on their existence for lattices corresponding to \mathcal{W}_a^{199} and \mathcal{W}_b^{199} .

Sites in \mathcal{W}_a^{199} are invariant under a three-fold rotation, but the rotation axes are site-dependent. An SG symmetric spin-texture can be formed by polarizing spins along the corresponding axis on each site. Sites in \mathcal{W}_b^{199} are invariant up to lattice translation under

one of the two-fold screws, and so the spin-texture has the spins polarized along the corresponding screw axes. The spin-quantization axes are uniquely defined for sites in \mathcal{W}_a^{199} and \mathcal{W}_b^{199} (up to a global choice of up vs down), but to be self-contained we list them in table S2. The spin-quantization axes for \mathcal{W}_b^{199} are also shown in fig. S1.

We also clarify here a subtle point (though non-essential for our arguments): if the screws were 'intrinsically' non-symmorphic (NS), no site should be taken back to itself nor its lattice-translation images. This, however, is not the case for SG No. 199 as the screws are not intrinsic: given any of the screws, one can choose an origin such that the 'screw' factorizes into a point-group rotation followed by lattice translation. No. 199 is nonetheless NS because no common origin can be picked to render all space group elements symmorphic. SGs like No. 199, which are NS but do not contain any intrinsically NS element, are known as 'exceptional' NS SGs, and in fact there are only two of them out of the 230 SGs: No. 24 and No. 199.

table S2. Spin-quantization axes corresponding to the SG symmetric spin texture. The sites are labeled by l in the same order as they are listed in ITC (5). The axes are parameterized as $\hat{n}_l = (\sin \theta_l \cos \phi_l, \sin \theta_l \sin \phi_l, \cos \theta_l)$, and we let $\theta_{[111]} = \cos^{-1}(1/\sqrt{3})$.

(a) \mathcal{W}_a^{199}			(b) \mathcal{W}_b^{199}		
l	θ_l	ϕ_l	l	θ_l	ϕ_l
1	$\theta_{[111]}$	$\pi/4$	1	$\pi/2$	0
2	$\theta_{[111]}$	$-3\pi/4$	2	$\pi/2$	π
3	$\pi - \theta_{[111]}$	$3\pi/4$	3	$\pi/2$	$\pi/2$
4	$\pi - \theta_{[111]}$	$-\pi/4$	4	$\pi/2$	$-\pi/2$
			5	0	0
			6	π	0

Little group irreducible representations

In table S3 we list the symmetry eigenvalues of the different irreducible representations of the little group at high symmetry momenta $\Gamma = (0,0,0)$, $H = (2\pi,0,0)$ and $P = (\pi,\pi,\pi)$. The set of isolated four bands forming feQBI corresponds to $\rho_{\Gamma}^{(2b)} \oplus \rho_{\Gamma}^{(2c)}$ at Γ and $\rho_P^{(1a)} \oplus \rho_P^{(3a)}$ at P . Irreps at other high symmetry momenta are fixed once these are specified.

table S3. Symmetry eigenvalues of the irreducible little group representations at high-symmetry momenta. We denote $\omega = e^{-i2\pi/3}$.

el.	(a) $\Gamma = (0,0,0)$ and $H = (2\pi,0,0)$:			(b) $P = (\pi,\pi,\pi)$:			
	$\rho_{\Gamma}^{(2a)}$	$\rho_{\Gamma}^{(2b)}$	$\rho_{\Gamma}^{(2c)}$	$\rho_P^{(1a)}$	$\rho_P^{(1b)}$	$\rho_P^{(1c)}$	$\rho_P^{(3a)}$
(1)	{1,1}	{1,1}	{1,1}	1	1	1	{1,1,1}
(2)	{i,-i}	{i,-i}	{i,-i}	-1	-1	-1	{-1,1,1}
(3)	{i,-i}	{i,-i}	{i,-i}	-1	-1	-1	{-1,1,1}
(4)	{i,-i}	{i,-i}	{i,-i}	-1	-1	-1	{-1,1,1}
(5)	{- ω , - ω^* }	{-1, - ω }	{-1, - ω^* }	-1	- ω	- ω^*	{-1, - ω , - ω^* }
(6)	{- ω , - ω^* }	{-1, - ω }	{-1, - ω^* }	-1	- ω	- ω^*	{-1, - ω , - ω^* }
(7)	{- ω , - ω^* }	{-1, - ω }	{-1, - ω^* }	-1	- ω	- ω^*	{-1, - ω , - ω^* }
(8)	{- ω , - ω^* }	{-1, - ω }	{-1, - ω^* }	-1	- ω	- ω^*	{-1, - ω , - ω^* }
(9)	{ ω , ω^* }	{1, ω^* }	{1, ω }	1	ω^*	ω	{1, ω , ω^* }
(10)	{ ω , ω^* }	{1, ω^* }	{1, ω }	-1	- ω^*	- ω	{-1, - ω , - ω^* }
(11)	{ ω , ω^* }	{1, ω^* }	{1, ω }	-1	- ω^*	- ω	{-1, - ω , - ω^* }
(12)	{ ω , ω^* }	{1, ω^* }	{1, ω }	-1	- ω^*	- ω	{-1, - ω , - ω^* }

feQBI tight-binding examples

Model given in Eq. 1 of main text

One can deduce the transformation of tight-binding (TB) degrees of freedom by assigning them to some actual locations in real space. In Eq. 1 of main text, we assume the sites have coordinates in \mathcal{W}_6^{199} at $x=1/8$, with a single s -orbital on each site. Note that the TB model is chosen such that it contains the irreps needed to realize feQBI, but feQBI is possible in any TB models that contains the irreps required.

We label the sites (1-6) in the same order as they appear in ITC (5) (left-right). In writing their coordinates as $\vec{r} = \vec{x} + \vec{r}^l$ with \vec{x} a lattice vector, \vec{r}^l depends on the choice of the unit cell. Here, we take the primitive lattice vectors as $\vec{a}_1 = (1/2, 1/2, 1/2)$, $\vec{a}_2 = (0, 1, 0)$ and $\vec{a}_3 = (0, 0, 1)$, and choose \vec{r}^l such that \vec{r}^l are contained inside the parallelepiped defined by the three primitive lattice vectors. With this choice of unit cell, the coordinates are given by

$$\begin{aligned}\vec{r}^1 &= (1/8, 1, 1/4); & \vec{r}^2 &= (3/8, 1, 3/4); \\ \vec{r}^3 &= (1/4, 9/8, 1); & \vec{r}^4 &= (1/4, 7/8, 1/2); \\ \vec{r}^5 &= (0, 1/4, 1/8); & \vec{r}^6 &= (0, 3/4, 3/8).\end{aligned}\tag{S1}$$

The transformation of the TB basis is parameterized by writing $g(\vec{r}^l) = n_i \vec{a}_i + \vec{r}^l$, where $\{n_i\}$ is a triplet of integers. While this is readily computable, in table S4 we tabulate the transformation of site l as $(l'; n_1, n_2, n_3)$ under the symmetry elements.

table S4. Transformation of tight-binding sites under the symmetry elements (el.). Sites are labeled by l and \bar{n} denotes $-n$.

el. \ l	1	2	3	4	5	6
(1)	(1;0 0 0)	(2;0 0 0)	(3;0 0 0)	(4;0 0 0)	(5;0 0 0)	(6;0 0 0)
(2)	(2;0 $\bar{2}$ 0)	(1;0 $\bar{2}$ 1)	(4;0 $\bar{2}$ 1)	(3;0 $\bar{2}$ 0)	(5;1 $\bar{1}$ 0)	(6;1 $\bar{2}$ 0)
(3)	(2; $\bar{1}$ 10)	(1; $\bar{1}$ 10)	(3; $\bar{1}$ 1 $\bar{1}$)	(4; $\bar{1}$ 10)	(6;0 0 0)	(5;0 1 0)
(4)	(1;1 $\bar{2}$ 1)	(2;1 $\bar{2}$ 2)	(4;1 $\bar{2}$ 2)	(3;1 $\bar{2}$ 2)	(6;1 $\bar{1}$ 1)	(5;1 $\bar{1}$ 1)
(5)	(3;0 $\bar{1}$ 0)	(4;1 $\bar{1}$ 0)	(5;2 $\bar{1}$ 0)	(6;1 $\bar{1}$ 0)	(1;0 $\bar{1}$ 0)	(2;0 $\bar{1}$ 0)
(6)	(4;1 $\bar{1}$ 2)	(3;2 $\bar{2}$ 3)	(6;3 $\bar{2}$ 3)	(5;2 $\bar{1}$ 2)	(1;1 $\bar{1}$ 1)	(2;1 $\bar{1}$ 2)
(7)	(4;0 $\bar{1}$ 1)	(3; $\bar{1}$ 11)	(5; $\bar{1}$ 02)	(6;0 $\bar{1}$ 1)	(2;0 $\bar{1}$ 0)	(1;0 $\bar{1}$ 1)
(8)	(3; $\bar{1}$ 0 $\bar{1}$)	(4; $\bar{2}$ 10)	(6; $\bar{2}$ 10)	(5; $\bar{1}$ 10)	(2; $\bar{1}$ 00)	(1; $\bar{1}$ 00)
(9)	(5;2 $\bar{1}$ 1)	(6;2 $\bar{1}$ 1)	(1;2 $\bar{1}$ 1)	(2;1 $\bar{1}$ 1)	(3;0 $\bar{1}$ 1)	(4;1 $\bar{1}$ 1)
(10)	(6; $\bar{2}$ 11)	(5; $\bar{2}$ 21)	(2; $\bar{3}$ 21)	(1; $\bar{2}$ 11)	(3; $\bar{1}$ 00)	(4; $\bar{2}$ 11)
(11)	(6;3 $\bar{2}$ 2)	(5;3 $\bar{2}$ 2)	(1;3 $\bar{3}$ 2)	(2;2 $\bar{2}$ 2)	(4;1 $\bar{1}$ 1)	(3;2 $\bar{2}$ 2)
(12)	(5; $\bar{1}$ 01)	(6; $\bar{1}$ 11)	(2; $\bar{2}$ 11)	(1; $\bar{1}$ 11)	(4;0 $\bar{1}$ 0)	(3; $\bar{1}$ 10)

To construct a Hamiltonian H that is fully symmetric under SG \mathcal{G} , one can start from a single (non-symmetric) term H_0 , like the one given in Eq. 1 of main text, and take the summation $H = \sum_{g \in \mathcal{G}} g H_0 g^{-1}$. For reader's convenience, we give an explicit form of H in the momentum space here. To fix notation, we specify a generic term in a periodic Hamiltonian for SOC electrons as follows:

$$H_{\mathbf{k}}^{\delta\mathbf{x},l',\Delta,\lambda,l} = e^{-i\mathbf{k}\cdot\delta\mathbf{x}} f_{\mathbf{k}}^{l's'\dagger} (\Delta\delta_{s't} + i(\lambda \cdot \sigma)_{s't}) f_{\mathbf{k}}^{ls} + \text{h.c.} \quad (\text{S2})$$

where $\delta\vec{x}$ is also a lattice vector. In table S5, we specify the Hamiltonian by providing a list of all terms in this notation.

table S5. A full list of terms in the feQBI tight-binding example given in the main text. The terms are parameterized as in eq. S2.

$\vec{k}\cdot\delta\vec{x}$	l'	Δ	$\vec{\lambda}$	l
0	4	t	$(0,0,\lambda)$	1
0	3	t	$(0,0,\lambda)$	2
0	4	t	$(0,0,-\lambda)$	2
$-k_z$	3	t	$(0,0,-\lambda)$	1
$(k_x+k_y+k_z)/2$	6	t	$(\lambda,0,0)$	3
$(k_x+k_y+k_z)/2$	5	t	$(\lambda,0,0)$	4
0	6	t	$(-\lambda,0,0)$	4
k_y+k_z	5	t	$(-\lambda,0,0)$	3
$-(k_x+k_y+k_z)/2$	2	t	$(0,\lambda,0)$	5
0	1	t	$(0,\lambda,0)$	6
$-(k_x+k_y+k_z)/2$	2	t	$(0,-\lambda,0)$	6
$-k_y$	1	t	$(0,-\lambda,0)$	5

An alternative 'minimal' model

Since $\nu_{\min}^{\text{Band}} = 4$ for SG No. 199, the 'minimal' tight-binding model (corresponding to local Hamiltonians) should have at least eight bands. This is indeed possible by considering a pair of orbitals on each of the sites furnishing \mathcal{W}_a^{199} . However, to match the representation content required for forming a feQBI, the TB degrees of freedom have to transform in a more intricate manner under the SG symmetries.

To this end, note again that each site in \mathcal{W}_a^{199} is invariant under a three-fold rotation along a site-dependent axis, and hence it can pick-up an orbital phase of 1, $\omega = e^{-i2\pi/3}$ or ω^2 under the three-fold rotations. A spin-1/2 polarized along the three-fold rotation axis will also pick up a phase of $e^{-i2\pi/6}$ for spin- \uparrow and $e^{i2\pi/6}$ for spin- \downarrow . In particular, we consider a TB model formed by the (ω, \uparrow) and (ω^2, \downarrow) orbitals on each of the symmetry-related sites belonging to \mathcal{W}_a^{199} . Note that the two on-site orbitals also interchange under TR.

We again parametrize the TB model in a similar manner as in eq. S2, but here we use an unconventional basis for the Pauli matrices (corresponding to indices s and s'), namely we

write $\begin{pmatrix} f_{\bar{x}}^{l1\uparrow} & f_{\bar{x}}^{l2\uparrow} \end{pmatrix} = \begin{pmatrix} \tilde{f}_{\bar{x}}^{l\uparrow\uparrow} & \tilde{f}_{\bar{x}}^{l\downarrow\uparrow} \end{pmatrix} U(\theta_l, \phi_l)$, where $\tilde{f}_{\bar{x}}^{l\uparrow\uparrow}$ and $\tilde{f}_{\bar{x}}^{l\downarrow\uparrow}$ are respectively the

creation operators for the (ω, \uparrow) and (ω^2, \downarrow) orbitals on the l -th site in the unit cell with

coordinate \bar{x} , and $U(\theta_l, \phi_l)$ is the site-dependent unitary transformation relating the

crystalline z -axis to the SG symmetric spin-texture (table S2), i.e. had we picked the \uparrow and \downarrow states from the same orbital then $f_{\bar{x}}^{ls\uparrow}$ would just correspond to the creation operator

written in the basis of crystalline z -axis.

We consider a TB model with four sites in each unit cell starting with $\vec{r}^1 = (0,0,0)$. Similar to the previous example the coordinates \vec{r}^l for $l=1,\dots,4$ can then be determined from the SG symmetries (same choice of unit cell as before), with the sites labeled in the same order as in ITC. The terms in the eight-band TB Hamiltonian are tabulated in table S6. In particular, TR invariance of the Hamiltonian still requires Δ , $\vec{\lambda}$ to be real, although the Δ term is no longer spin-independent in this choice of basis. One can check that the system forms a feQBI when, say, $t_2'/t_1' = 2$. The corresponding electronic and entanglement bands are plotted in fig. S2.

table S6. Terms in an alternative eight-band feQBI tight-binding example.

$\vec{k} \cdot \delta \vec{x}$	l'	Δ	$\vec{\lambda}$	l
0	4	t_1'	(0,0,0)	1
0	3	t_1'	(0,0,0)	2
0	2	0	(0, t_1' , 0)	1
k_y	4	0	(0, t_1' , 0)	3
$(k_x - k_y - k_z)/2$	3	0	(0, 0, $-t_1'$)	1
$(-k_x + k_y - k_z)/2$	4	0	(0, 0, $-t_1'$)	2
$-k_z$	4	0	(0, 0, t_2')	1
$-k_z$	3	0	(0, 0, t_2')	2
$-k_y$	2	0	($-t_2'$, 0, 0)	1
0	4	0	(t_2' , 0, 0)	3
$-(k_x + k_y + k_z)/2$	3	t_2'	(0,0,0)	1
$(k_x + k_y - k_z)/2$	4	t_2'	(0,0,0)	2

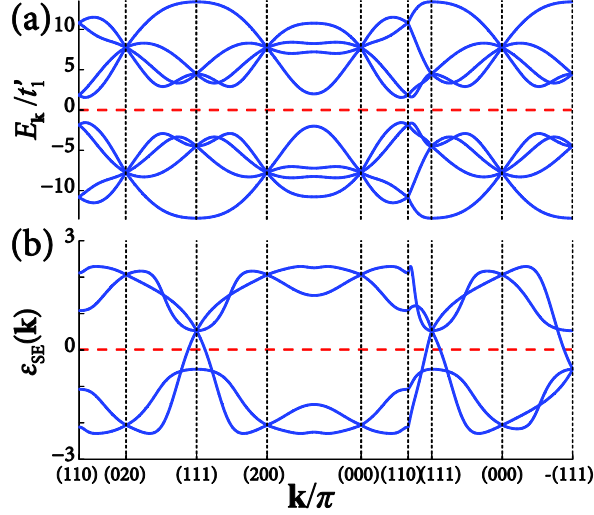


fig. S2. Energy and entanglement band structure for an alternative feQBI example for SG No. 199. Note that the symmetry representation content is identical to the example given in the main text. (a) Band structure with $t_2/t_1 = 2$. The model has an extra 'sub-lattice' symmetry (i.e. there exists a unitary U such that $UH_{\vec{k}}U = -H_{\vec{k}}$) and hence the bands are symmetric about $E_{\vec{k}} = 0$, but this is purely an artifact of the simple TB model and is not essential. (b) Corresponding entanglement band structure.

Hyperkagome lattice and feQBI in the Wyckoff-mismatched space groups No. 214, 220 and 230

In this subsection we show that the simple TB model in Eq. 1 of main text can be used to establish the existence of feQBIs in all the four Wyckoff-mismatched SGs: No. 199, 214, 220 and 230. We reproduced in Table 1 of the main text the multiplicities of the Wyckoff positions for these four SGs. Note that not all $|\mathcal{W}_w^{\mathcal{G}}|$ are integer multiples of $|\mathcal{W}_a^{\mathcal{G}}|$ for these SGs.

To this end, we first focus on SG No. 214. As listed in Table 1, $|\mathcal{W}_a^{214}| = 4$ and so $\nu_{\min}^{\text{AI}} = 8$ for SG No. 214. Now we note that the coordinates listed in eq. S1 are chosen to coincide with \mathcal{W}_c^{214} . Recall that with only nearest-neighbour bonds, the system is in a hyperkagome structure and each site is four-coordinated. Demanding TR and spatial symmetries of SG No. 214, the symmetry allowed terms take the form

$$H = f_{\vec{x}}^{4s^\dagger} \left(t \delta_{s's} + i(\lambda_1 \sigma^z + \lambda_2 (\sigma^x - \sigma^y))_{s's} \right) f_{\vec{x}}^{1s} + \text{h.c.} + (\text{symmetry-related terms}). \quad (\text{S3})$$

Eq. 1 of main text corresponds to the special case when $\lambda_2 = 0$, and so it can just as well be regarded as an example of an insulating state in SG No. 214 with filling $\nu = 4 < 8$. This establishes the existence of feQBI for SG No. 214. For completeness, we also plot in fig. S3 the phase diagram of the system described by eq. S3 at filling $\nu = 4$.

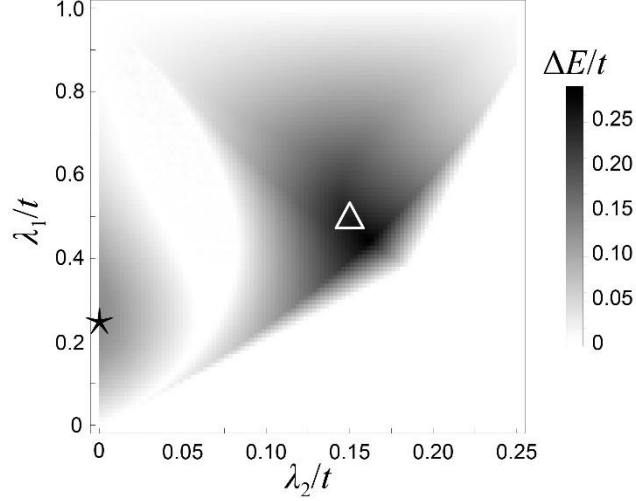


fig. S3. Plot of band gap ΔE for the hyperkagome model in eq. S3 at filling $\nu = 4$. For each pixel of the plot, ΔE is determined by sampling 30×10^3 momentum points along the high symmetry lines and in the first Brillouin zone respectively. \star corresponds to the system for Fig. 1(e,f) of the main text and Δ corresponds to that of fig. S4.

Next we consider the centrosymmetric SG No. 230, which can be viewed as SG No. 214 supplemented with spatial inversion. In particular, \mathcal{W}_c^{230} is the union of \mathcal{W}_c^{214} and \mathcal{W}_d^{214} , which are inversion-copy of each other. Consequentially, one can simply take the TB model in eq. S3 together with its inversion copy to construct a TB model symmetric under SG No. 230 (defined on two inter-penetrating hyperkagome lattices that are decoupled). Hence one can construct a TR symmetric insulator with SG No. 230 at $\nu = 8$. Since $8 < 2|\mathcal{W}_a^{230}| = 16$, this is also a feQBI.

Finally, we note that SG No. 220 is a subgroup of No. 230. In particular, $8 < 2|\mathcal{W}_a^{220}| = 12$ and so the same model constructed for No. 230 is also a feQBI example for No. 220.

Strong and weak indices of feQBI examples

The strong and weak indices were found by computing the \mathbb{Z}_2 indices for the six TR-symmetric planes spanned by two of the reciprocal lattice vectors in the Brillouin zone containing either Γ or $\vec{G}_i/2$ (where \vec{G}_i is the remaining reciprocal lattice vector not spanning the plane). The strong index was found to be $\nu_0 = 1$ and 0 respectively for the SG No. 199 feQBI models in Eq. 1 of main text and the one specified in table S6, while both of them have weak indices characterized by the vector $\vec{G}_\nu = \frac{1}{2} \nu_i \vec{G}_i = 2\pi \hat{x}$. As such, these models actually feature surface states (on the appropriate surfaces), even though they are not required by the filling-enforced nature emphasized in this work.

We note that, however, it is not necessary for a feQBI to simultaneously possess nontrivial \mathbb{Z}_2 indices. For instance, consider the inter-penetrating hyperkagome model mentioned as feQBI of SGs No. 220 and 230. The various \mathbb{Z}_2 indices are simply given by twice of the corresponding indices of the model in Eq. 1 of main text, and therefore must be trivial.

As another example, observe that fig. S3 features two 'islands' of insulating phases, separated by a gapless region. This is not a coincidence. The island marked by \star corresponds to the strong TI model given in the main text, and the one marked by Δ is in fact neither a strong nor weak TI. As such the mentioned gapless phase between the two islands should actually feature a nodal semi-metal. We plot in fig. S4 the surface band structures of Δ on various surfaces, all of which are gapped.

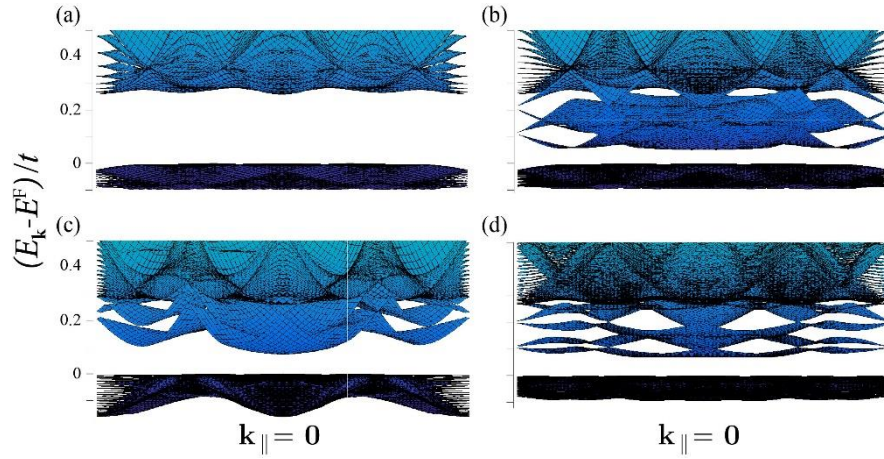


fig. S4. Plot of surface band structure against the surface crystal momentum \vec{k}_{\parallel} for the model in eq. S3. We take $\lambda_1/t = 0.5$, $\lambda_2/t = 0.15$ and E^F denotes the bulk Fermi energy. Slabs with thickness of 20 surface-adapted unit cells are used and results for different surfaces, corresponding to different surface normal \hat{n} , are shown. Note that with open boundary conditions, there are surface states but they do not traverse the bulk gap. (a) Periodic boundary condition for $\hat{n} = \hat{z}$. (b) Open boundary condition for $\hat{n} = \hat{z}$. (c) Open boundary condition for $\hat{n} \sim \hat{y} + \hat{z}$. (d) Open boundary condition for $\hat{n} \sim \hat{x} + \hat{y} + \hat{z}$.

Hypothetical structure for spin-orbit-coupled hyperkagome material $\text{Na}_3\text{Ir}_3\text{O}_8$

In this appendix we point out the observation that the experimentally synthesized hyperkagome material $\text{Na}_3\text{Ir}_3\text{O}_8$ (Na-338) is in close proximity to a feQBI phase, and can point to promising avenues for the experimental realization of feQBIs.

Na-338 can be regarded as a hole-doped version of Na-438, a Mott-insulating hyperkagome material well-known as a spin-liquid candidate (17). In reality Na-338 crystallizes in SG No. 213 (19), which is a primitive version of SG No. 214. The structure of the atoms are listed in table (S7) (adapted from Ref. (19)).

table S7. Measured structure of $\text{Na}_3\text{Ir}_3\text{O}_8$ by Takayama et al. (19). The structure is in SG No. 213 and we use the notation in ITC (5).

Atom	Wyckoff	Free Parameter	Representative
Ir	12d	$y = -0.113$	(0.613, 0.863, 5/8)
O1	8c	$x = 0.114$	(0.114, 0.114, 0.114)
O2	24e	(x, y, z)	(0.136, 0.907, 0.919)
Na1	4b	-	(7/8, 7/8, 7/8)
Na2	8c	$x = 0.257$	(0.257, 0.257, 0.257)

Due to the strong SOC of Iridium and crystal field splitting coming from the local environment, the relevant states near the Fermi level can be (roughly) modeled after an effective $J_{\text{eff}} = 1/2$ Kramers pair centered at the Ir sites (18). This gives rise to 24 relevant energy bands around the Fermi level with an electron filling of $\nu = 8$. (Note that in this picture, we are regarding the other 48 bands arising from the $J_{\text{eff}} = 3/2$ states of Ir as separated in energy and fully filled, contributing to 'core electron states'.)

While Na-338 is semi-metallic in reality (19), here we consider a hypothetical structure of it in which the atom positions are modified to 'enrich' the spatial symmetries from SG~No. 213 (simple cubic) to No.~214 (body-centered cubic). In particular, we change the free parameter associated with Ir in table S7 from $y = -0.113$ to $y = 0$, putting the Iridium atoms in \mathcal{W}_c^{214} .

A possible assignment of the other atoms are provided in table S8.

table S8. 'Symmetry-enriched' hypothetical structure of $\text{Na}_3\text{Ir}_3\text{O}_8$ in SG No. 214.

Atom	Wyckoff	Free Parameter	Representative
Ir	12c	-	(0, 1/4, 1/8)
O1	8a	-	(1/8, 1/8, 1/8)
O2	24h	$y = 1/4$	(0, 1/8, 1/4)
Na	12d	-	(0, 1/4, 5/8)

In promoting the bravais lattice from simple cubic in SG No. 213 to body-centered cubic in No. 214, the electron filling per primitive unit cell is halved. Retaining only nearest-neighbour bonds, the system can now be effectively described by eq. S3 with $\nu = 4$ and serves as a feQBI example if the parameters λ_1 and λ_2 lie in the insulating phase indicated in fig. S3.

Note that in this discussion we only intend to give experimental context to feQBIs, instead of proposing realistic material candidates. In particular, the 'oxygen cage' is significantly distorted from the ideal octahedron form in the structure tabulated in table S8, and hence whether the effective spin-1/2 picture still holds or not deserves scrutiny. Nonetheless, we also note that the site-symmetry group for \mathcal{W}_c^{214} is the crystallographic point-group D_2 , which has only one 2-dimensional spinful representation. As such, as long as one can identify a Kramers doublet living on the sites of \mathcal{W}_c^{214} and well isolated in energy from other states, the system is described by eq. S3 when restricted to nearest-neighbour bonds.

Discussions on the SE cut

General discussion on time-reversal symmetry

Consider an electronic system with particle number conservation. Let the total number of particles N be even and $|\Psi\rangle$ be a TR symmetric many-body state. We fix the phase

ambiguity such that $\hat{T}|\Psi\rangle = |\Psi\rangle$. Consider a basis $\{|i\rangle\}$ for sub-system \uparrow and $\{|\bar{i}\rangle\}$ for \downarrow .

In this basis, the ground state can be expanded as

$$|\Psi\rangle = \sum_{\bar{i}} M_{\bar{i}} |i\rangle |\bar{j}\rangle \quad (\text{S4})$$

Generally, M is a rectangular matrix. Since TR exchanges \uparrow and \downarrow , however, M here is in particular square. Singular-value-decomposition simply gives $M = W\lambda V^\dagger$, where W and V are unitary, and λ is diagonal and positive semi-definite. The Schmidt states in this basis are given by

$$|\Psi\rangle = \sum_{\alpha} \lambda_{\alpha} (|i\rangle W_{i\alpha}) (|\bar{j}\rangle V_{\bar{j}\alpha}^*) = \sum_{\alpha} \lambda_{\alpha} |\alpha\rangle_{\uparrow} |\alpha\rangle_{\downarrow}, \quad (\text{S5})$$

and in the same basis the reduced density matrices are $\rho_{\uparrow} = W\lambda^2 W^\dagger = MM^\dagger$ and

$\rho_{\downarrow} = V^* \lambda^2 V^T = M^T M^*$. Applying TR operator \hat{T} ,

$$|\Psi\rangle = \sum_{\alpha} \lambda_{\alpha} (\hat{T}|\alpha\rangle_{\uparrow}) (\hat{T}|\alpha\rangle_{\downarrow}) = \sum_{\alpha} \lambda_{\alpha} (|\alpha_{\hat{T}}\rangle_{\downarrow}) (|\alpha_{\hat{T}}\rangle_{\uparrow}) \quad (\text{S6})$$

one sees that the two Schmidt states $|\alpha\rangle_{\uparrow}$ and $|\alpha_{\hat{T}}\rangle_{\uparrow}$ are degenerate in the entanglement

spectrum. Note that while \hat{T} itself is anti-unitary, the map relating the ' \uparrow ' Schmidt states with the ' \downarrow ' Schmidt state is also anti-unitary. Altogether, TR becomes a unitary symmetry on the entanglement Hamiltonian.

To see this more explicitly, let TR transform the basis by

$$\hat{T}|i\rangle = |\bar{i}\rangle U_{\bar{i}}^{\hat{T}}; \quad \hat{T}|\bar{i}\rangle = |i\rangle \bar{U}_{\bar{i}}^{\hat{T}} \quad (\text{S7})$$

where the unitary matrices $U^{\hat{T}}$ and $\bar{U}^{\hat{T}}$ satisfy

$$\bar{U}^{\hat{T}} U^{\hat{T}} = (-1)^{\hat{N}} \quad (\text{S8})$$

as required by $\hat{T}^2 = (-1)^{\hat{N}}$. TR invariance of $\hat{T}|\Psi\rangle = |\Psi\rangle$ implies

$$M = \bar{U}^{\hat{T}} M^\dagger (U^{\hat{T}})^T \Rightarrow \rho_{\uparrow} = U^{\hat{T}} \rho_{\downarrow}^* U^{\hat{T}\dagger}. \quad (\text{S9})$$

One can bring ρ_{\downarrow} back to ρ_{\uparrow} using a 'spectral flattened' version of M : $\tilde{M} = WV^\dagger$. See that

$$\tilde{M}^\dagger \rho_{\uparrow} \tilde{M} = W^* \lambda^2 W^T = \rho_{\downarrow}^*, \quad (\text{S10})$$

so altogether

$$\rho_{\uparrow} = (U^{\hat{T}} \tilde{M}^\dagger) \rho_{\uparrow} (\tilde{M} U^{\hat{T}\dagger}) \quad (\text{S11})$$

i.e. TR is realized as a unitary symmetry on the entanglement Hamiltonian, as claimed.

In particular, since $[\hat{N}, \hat{T}] = 0$, we also have

$$\hat{N} (|\alpha_{\hat{T}}\rangle_{\uparrow}) = \hat{T} \hat{N} |\alpha\rangle_{\downarrow} = (N - N_{\alpha\uparrow}) (|\alpha_{\hat{T}}\rangle_{\uparrow}) \quad (\text{S12})$$

and hence the charges of the paired states are symmetric about $N/2$, i.e. TR is manifested in a 'particle-hole' manner. Note that since TR is now realized unitarily, a state with charge $N/2$ can be paired with itself under TR.

To illustrate the ideas discussed above, we provide here a simple illustrative example.

Consider a two-site system with a particular TR symmetric state

$$|\Psi\rangle = (\alpha f_{1\uparrow}^\dagger f_{1\downarrow}^\dagger + \beta(\gamma f_{1\uparrow}^\dagger f_{2\downarrow}^\dagger - \gamma^* f_{1\downarrow}^\dagger f_{2\uparrow}^\dagger) + \delta(\varepsilon f_{1\uparrow}^\dagger f_{2\uparrow}^\dagger + \varepsilon^* f_{1\downarrow}^\dagger f_{2\downarrow}^\dagger)) |0\rangle, \quad (\text{S13})$$

and under TR, $f_{i\uparrow}^\dagger \rightarrow f_{i\downarrow}^\dagger$ and $f_{i\downarrow}^\dagger \rightarrow -f_{i\uparrow}^\dagger$. Hence

$$\hat{T} |\Psi\rangle = (\alpha^* f_{1\uparrow}^\dagger f_{1\downarrow}^\dagger + \beta^*(\gamma f_{1\uparrow}^\dagger f_{2\downarrow}^\dagger - \gamma^* f_{1\downarrow}^\dagger f_{2\uparrow}^\dagger)) |0\rangle + \delta^*(\varepsilon f_{1\uparrow}^\dagger f_{2\uparrow}^\dagger + \varepsilon^* f_{1\downarrow}^\dagger f_{2\downarrow}^\dagger) |0\rangle. \quad (\text{S14})$$

Choosing the global phase such that $\hat{T} |\Psi\rangle = |\Psi\rangle$, we take $\alpha, \beta, \delta \in \mathbb{R}$.

The reduced density matrix obtained by tracing out occupancy states with label \downarrow has two degenerate eigenvalues of $\delta^2 |\varepsilon|^2$. These two Schmidt states, having charge 0 and 2

respectively, form a TR pair. The remaining 2-dimensional block is (in the basis of $f_{1\uparrow}^\dagger |0\rangle_{\uparrow}$

and $f_{2\uparrow}^\dagger |0\rangle_{\uparrow}$):

$$(\rho^\uparrow)_{2\times 2} = \begin{pmatrix} \alpha^2 + \beta^2 |\gamma|^2 & \alpha\beta\gamma \\ \alpha\beta\gamma^* & \beta^2 |\gamma|^2 \end{pmatrix} \quad (\text{S15})$$

The corresponding Schmidt weights are

$$\lambda_{\pm}^2 = \frac{\alpha^2}{2} + \beta^2 |\gamma|^2 \pm \alpha \sqrt{\frac{\alpha^2}{4} + \beta^2 |\gamma|^2} \quad (\text{S16})$$

which are generally non-degenerate, and each state is paired with itself under TR. This is allowed since they have charge $1=2/2$.

General discussion on space group symmetries

The SE cut is defined to partition degrees of freedom by their spin-label \uparrow, \downarrow , which are picked with respect to some quantization axes. In the presence of SOC, the spin states on different sites are also related by SG symmetries. Therefore, to ensure the SE cut is SG symmetric we must carefully choose the spin quantization axes in a site-dependent fashion.

A sufficient condition for the SE cut to respect all SG symmetries is the existence of SG-symmetric spin-texture, i.e. the spins can be polarized in a site-dependent fashion while preserving all the SG symmetries. Equivalently, we demand the existence of site-dependent spin-quantization axes for which any spatial symmetries either rotates the spin about the axis, or takes the site to some other site.

Generally speaking, such SG-symmetric spin-textures may not exist for a given lattice realization of a space group: whether or not they can be defined depends on the site-symmetry groups of the sites in the lattice. Since a generic point in space, belonging to the general Wyckoff position, is never taken back to itself under any SG element, the only possible obstruction comes from high-symmetry points (corresponding to high-symmetry Wyckoff positions) where any choice of spin-polarization breaks some site symmetries.

Nonetheless, as long as one is concerned about the space-group symmetries, but not the specific lattice realization of the system, any obstruction to defining an SG symmetric spin texture is largely technical. Intuitively, in the continuum it should be possible to adiabatically 'punch-out' the high-symmetry points without changing the phase. More concretely, one can always 'split up' a high-symmetry orbital into a small set of orbitals in the vicinity of the

high-symmetry point in order to avoid any obstruction. In other words, one can approximate any desired orbitals on a lattice site by effective 'molecular orbitals' on sites belonging to the lower-symmetry Wyckoff positions.

We also note that if the site-symmetry group is one of the 27 non-cubic crystallographic point groups, then all SG symmetries can be regarded as symmetries of the entanglement Hamiltonian (even when SG-symmetric spin-texture cannot be defined). This is due to the existence of a 'primary rotation axis' on the sites: for these 27 point groups, a spin polarized along the primary rotation axis is either flipped or left invariant (up to a phase) by any symmetry operations. An SG symmetry is then realized as an anti-unitary or unitary symmetry on the entanglement Hamiltonian depending on whether it flips the spin or not. In particular, we note that this is true for all the Wyckoff positions for the four Wyckoff-mismatched space groups.

Single-particle entanglement Hamiltonian

In the following subsections we specialize our discussion to free electron problems.

Due to Wick's theorem, the ground state entanglement spectrum of a free fermion system partitioned into A and \bar{A} is completely captured by the single-particle correlation matrix $C_{ij} = \langle \Psi | f_i^\dagger f_j | \Psi \rangle$, where $|\Psi\rangle$ is the many-body ground state and $i, j \in A$ (8-11). Since the spin-orbital entanglement cut preserves spatial symmetries, and in particular translation invariance, we can focus on correlation functions evaluated at a fixed momentum \vec{k} . This is related to the filled-band projector $\mathcal{P}_{\vec{k}}$ by $C_{\vec{k};\alpha\beta} = (\mathcal{P}_{\vec{k}}^T)_{\alpha\beta}$, where α, β are now collective indices for basis, orbitals and spin degrees of freedom, and run from $1, \dots, 2m$. In a proper choice of basis, the first m entries of $\mathcal{P}_{\vec{k}}$ correspond to the spin 'up' sector in the SE cut, and the $m \times m$ restricted correlation matrix is simply

$$C_{\vec{k}}^{\uparrow} = \begin{pmatrix} \mathbf{1}_{m \times m} & \mathbf{0}_{m \times m} \end{pmatrix} \mathcal{P}_{\vec{k}}^T \begin{pmatrix} \mathbf{1}_{m \times m} \\ \mathbf{0}_{m \times m} \end{pmatrix} \quad (\text{S17})$$

$C_{\vec{k}}^{\downarrow}$ is similarly defined. The definition is, of course, basis independent - a basis

transformation of $\mathcal{P}_{\vec{k}}$ is always accompanied by a corresponding transformation of the

rectangular matrix projector. Since $h_{\text{SE}}(\vec{k})$ is completely determined by $C_{\vec{k}}^{\uparrow}$, we focus on the properties of $C_{\vec{k}}^{\uparrow}$ in the following.

As $C_{\vec{k}}^{\uparrow}$ is a product of projectors, we have $\text{eig}(C_{\vec{k}}^{\uparrow}) \in [0,1]$. A (many-body) Schmidt state $|\lambda\rangle$ with charge N_{λ} is formed by populating N_{λ} single particle eigenstates $|c_i\rangle$ of the full ‘correlation Hamiltonian’ $C^{\uparrow} = \bigoplus_{\vec{k}} C_{\vec{k}}^{\uparrow}$. The eigenvalues of the reduced density matrix of such a state is a product over the eigenvalues of the occupied (occ.) and unoccupied (unocc.) states (8-11):

$$\lambda^2 = \prod_{i \in \text{occ.}} c_i \prod_{j \in \text{unocc.}} (1 - c_j) \quad (\text{S18})$$

and hence the highest-weight Schmidt states are formed by filling all states of C^{\uparrow} with $c_i > 0.5$, i.e. in this language one should think of filling the bands of C^{\uparrow} from above, not below, and the effective ‘chemical potential’ is 0.5. Note that the single-particle entanglement energies are related to c_i here by $\varepsilon_i = \log(c_i^{-1} - 1)$. In particular, if there are states with $c^i = 0.5$, they contribute to λ in the same way whether they are filled or not, and corresponds to degeneracy in the entanglement ground state. Note also that due to particle-hole character of the TR symmetry on the entanglement spectrum, the highest weight Schmidt state, if unique, must have a charge corresponding to half of the total physical charge.

Symmetry properties of the single-particle entanglement Hamiltonian

Recall that a single-particle Hamiltonian symmetric under a spatial symmetry g satisfies

$$U_{\vec{k}}^{g\dagger} H_{\vec{k}} U_{\vec{k}}^g = H_{g^{-1}(\vec{k})} \quad (\text{S19})$$

where $U_{\vec{k}}^g$ is a unitary. The notion of a spatially symmetric spin-texture implies that on each site, one can specify a spin quantization axis such that the two spin eigenstates are decoupled under all spatial symmetries. This implies there exists a \vec{k} -independent unitary matrix \mathcal{W}_g such that

$$\mathcal{W}_S U_k^g \mathcal{W}_S^\dagger = \begin{pmatrix} U_k^{g\uparrow} & 0 \\ 0 & U_k^{g\downarrow} \end{pmatrix} \quad (\text{S20})$$

For simplicity, in the following we assume we work with such a basis in mind such that we already have $U_k^g = U_k^{g\uparrow} \oplus U_k^{g\downarrow}$. Since the band projector satisfies

$$\mathcal{P}_k = U_k^{g\uparrow} \mathcal{P}_{g^{-1}(\vec{k})} U_k^g \quad (\text{S21})$$

the restricted correlation matrix transforms as

$$C_k^{\uparrow} = \left(U_k^{g\uparrow} \right)^T C_{g^{-1}(\vec{k})}^{\uparrow} \left(U_k^{g\uparrow} \right)^* \quad (\text{S22})$$

i.e. it transforms as a spin-polarized system with the same SG symmetries.

It remains to show how the original TR symmetry is manifested in C_k^{\uparrow} . Note that for the

original Hamiltonian, TR symmetry implies $H_{\vec{k}} = U_T H_{-\vec{k}}^* U_T^\dagger$, and therefore $\mathcal{P}_{-\vec{k}} = U_T^T \mathcal{P}_{\vec{k}}^* U_T^*$.

In the basis of eq. S17, one simply has $U_T = -i\sigma^y \otimes 1_{m \times m}$, and therefore $C_k^{\uparrow} = \left(C_k^{\downarrow} \right)^*$. Using

the properties of the projectors and the duality discussed in Ref. (10), one sees that if

$c_k^i \in (0,1)$ is an eigenvalue of $H_k^{C\uparrow}$, then $1 - c_k^i$ is an eigenvalue of $C_{-\vec{k}}^{\uparrow}$, i.e. TR is now

manifested as a 'particle-hole' symmetry between $h_{\text{SE}}(\vec{k})$ and $h_{\text{SE}}(-\vec{k})$ (Fig. 1B of main text

and fig. S2b). More explicitly, suppose $C_k^{\uparrow} \psi = \psi c_k$, and let

$$\tilde{\psi} = (0 \quad 1) \mathcal{P}_k^T \begin{pmatrix} \psi \\ 0 \end{pmatrix} \quad (\text{S23})$$

One can then verify $C_k^{\downarrow} \tilde{\psi} = (1 - c_k) \tilde{\psi}$. Hence, as long as $\tilde{\psi} \neq 0$, it is an eigenvector of $H_k^{C\downarrow}$

with eigenvalue $1 - c_k$. In addition, one can check that $\tilde{\psi} = 0$ implies $c_k = 0$ or 1, so any

$c_k \in (0,1)$ is paired with a $c_{-\vec{k}} = 1 - c_k$, i.e. translating this relation into the spectrum of

$h_{\text{SE}}(\vec{k})$, TR is reflected as a particle-hole like symmetry with $\varepsilon_{\text{SE}}(\vec{k}) = -\varepsilon_{\text{SE}}(-\vec{k})$.

Proof of gaplessness of entanglement Hamiltonian for $\nu = 4$ feQBI symmetric under time-reversal and space group No. 199

We argue by contradiction. Assume the many-body entanglement Hamiltonian is gapped with a unique ground state. Because TR acts as a particle-hole symmetry, the filling of the entanglement ground state must be half the physical filling, $\nu_{\text{SE}} = \nu / 2 = 2$, implying bands 1, 2 lie isolated below the entanglement Fermi level $\varepsilon^{\text{F}} = 0$

$$\varepsilon_{\text{SE}}^{(1)}(\vec{k}) \leq \varepsilon_{\text{SE}}^{(2)}(\vec{k}) < 0 < \varepsilon_{\text{SE}}^{(3)}(\vec{k}) \leq \varepsilon_{\text{SE}}^{(4)}(\vec{k}). \quad (\text{S24})$$

However, we find that at $\vec{k} = \text{P} \equiv (\pi, \pi, \pi)$ the four bands must transform under a 1D and 3D irreps. It follows from the fact that the collection of irreps at P carried by the ν entanglement bands must be the *same* as those of the ν physical bands. This is because h_{SE} is unitarily related to C , the occupied band projector further projected onto the $\uparrow\uparrow$ space; the latter projection respects the SG symmetries and so leaves irreps unchanged.

The feQBI at P has one 1D irrep and one 3D irrep, and this is a robust property of the system: the counting $4 = 1+3$ cannot be altered without closing the gap, and is independent of any particular tight-binding model used. This forces $\varepsilon^{(2)}(\text{P}) = \varepsilon^{(3)}(\text{P})$, which is incompatible with an entanglement gap and hence a contradiction.